Waste Management 58 (2016) 230–240

Contents lists available at ScienceDirect

Waste Management

journal homepage: www.elsevier.com/locate/wasman

# Kinetic analysis of manure pyrolysis and combustion processes

M. Fernandez-Lopez, G.J. Pedrosa-Castro, J.L. Valverde, L. Sanchez-Silva *

*Department of Chemical Engineering, University of Castilla-La Mancha, Ciudad Real, Spain*

ARTICLE INFO

*Article history:*
Received 30 May 2016
Revised 22 August 2016
Accepted 25 August 2016
Available online 29 August 2016

*Keywords:*
Manure
Pyrolysis
Combustion
TGA
Model-free methods
DAEM

ABSTRACT

Due to the depletion of fossil fuel reserves and the environmental issues derived from their use, biomass seems to be an excellent source of renewable energy. In this work, the kinetics of the pyrolysis and combustion of three different biomass waste samples (two dairy manure samples before (Pre) and after (Dig R) anaerobic digestion and one swine manure sample (SW)) was studied by means of thermogravimetric analysis. In this work, three iso-conversional methods (Friedman, Flynn-Wall-Ozawa (FWO) and Kissinger-Akahira-Sunose (KAS)) were compared with the Coats-Redfern method. The $E_a$ values of devolatilization stages were in the range of 152–170 kJ/mol, 148–178 kJ/mol and 156–209 kJ/mol for samples Pre, Dig R and SW, respectively. Concerning combustion process, char oxidation stages showed lower $E_a$ values than that obtained for the combustion devolatilization stage, being in the range of 140–175 kJ/mol, 178–199 kJ/mol and 122–144 kJ/mol for samples Pre, Dig R and SW, respectively. These results were practically the same for samples Pre and Dig R, which means that the kinetics of the thermochemical processes were not affected by anaerobic digestion. Finally, the distributed activation energy model (DAEM) and the pseudo-multi component stage model (PMSM) were applied to predict the weight loss curves of pyrolysis and combustion. DAEM was the best model that fitted the experimental data.



## 1. Introduction

It is well known that fossil fuel reserves will be completely depleted in the near future, being their consumption rate about 91 million barrels per day of oil and 9 billion cubic metres per day of natural gas (BP, 2013). In this context, biomass is considered to be an important source of renewable and clean energy, reducing $CO_2$ emission because of its carbon–neutral nature. Among the different type of biomasses, livestock manure has been commonly used as fertilizer and landfill. However, these uses have to be changed due to land saturation with phosphorous and stricter regulations (Cao et al., 2015). Therefore, the utilization of manure for the waste-to-bioenergy generation could be a sustainable choice since it is considered a zero-cost feedstock (Fernandez-Lopez et al., 2015).

Regarding the processes available to obtain bioenergy from biomass, thermochemical conversion processes can be used for the transformation of dry biomasses into biofuels. Concretely, combustion is defined as the oxidation of biomass with air or under an oxidizing atmosphere with excess of oxygen and pyrolysis can be defined as the degradation of the biomass by heating it in a non-oxidant atmosphere, leading to three different products: solid char, bio-oil and fuel gas.

Modelling these thermochemical processes is essential for understanding the behavior at industrial scale (Kantarelis et al., 2011). Furthermore, adequate models are necessary for the design and operation of conversion systems (Garcia-Maraver et al., 2015). Kinetics of mass loss is required for modelling the processes of pyrolysis, combustion and gasification (López-González et al., 2014). Experimental data obtained from thermogravimetric analysis (TGA) is needed for the kinetic evaluation and the thermochemical systems design (Tran et al., 2014).

Generally, there are two different types of methods for analyzing non-isothermal solid-state kinetic data obtained by TGA: model-fitting and model-free methods (Anca-Couce et al., 2014; Garcia-Maraver et al., 2015). Model-fitting methods consist of choosing the model which achieves the best fitting of the experimental data to obtain the kinetic parameters (activation energy and pre-exponential factor). On the other hand, model-free or iso-conversional methods are used to obtain the activation energy at a given extent of conversion without assuming or determining any reaction model (Vyazovkin et al., 2011; Slopiecka et al., 2012).

Numerous investigations have been performed in order to determine the kinetic of the biomass pyrolysis and combustion. Pyrolysis kinetics is the most studied one and different works can be found in a recent review (White et al., 2011). Furthermore,

* Corresponding author.
*E-mail address:* marialuz.sanchez@uclm.es (L. Sanchez-Silva).

http://dx.doi.org/10.1016/j.wasman.2016.08.027
0956-053X/

Slopiecka et al. (2012) studied the kinetic of the poplar wood slow pyrolysis using two isoconversional methods: Flynn-Wall-Ozawa (FWO) and Kissinger-Akahira-Sunose (KAS) ones. They concluded that the kinetic values obtained from the different methods were consistent and the FWO and KAS isoconversional methods, satisfactorily described the complexity of devolatilization step during pyrolysis process. Chen et al. (2011) investigated the kinetic behavior of microalgae *Chlorella vulgaris* combustion under different oxygen concentrations. They studied the kinetics using two iso-conversional methods (FWO and KAS) and observed that activation energy values increased with the oxygen concentration. Garcia-Maraver et al. (2015) evaluated the kinetic parameters during combustion of agricultural residues from olive trees using two model-free methods (FWO and KAS) and one model-fitting (Coats-Redfern). In this case, the values of the activation energy calculated by FWO and KAS were confirmed by Coats-Redfern method when a first order reaction was considered. Xu and Chen (2013) studied the thermal conversion characteristics and the kinetics of dairy and chicken manure pyrolysis. They used the Flynn-Wall method to obtain the activation energy. They concluded that the activation energy steeply varied with the extent of conversion, from 120 to 180 kJ/mol at a mass conversion of 0.2–0.4, followed by a relatively steady change at 0.4–0.65.

The objective of this study is to evaluate and compare different kinetic methods, such as model-fitting (Coats-Redfern approach) and model-free (Friedman, FWO and KAS) methods for the kinetics of some residual biomass (manure) pyrolysis and combustion processes. Moreover, to corroborate the kinetic analysis two home-made Excel Visual Basic applications based on both the distributed activation energy (DAEM) and pseudo-multi component stage models (PMSM) were developed. Unlike previous studies where only the devolatilization stage of pyrolysis and combustion processes was considered, in this work, the main stage of the pyrolysis process (devolatilization) and the two main stages of the combustion process (both devolatilization and char oxidation stages) were taking into account.

## 2. Materials and methods

### 2.1. Materials

Three biomasses from three different animal solid wastes (manure) coming from the region of Québec (Canada) were considered: one swine manure sample (SW) pretreated by a bio-drying process and two dairy manure samples before (Pre) and after (Dig R) anaerobic digestion. The biomasses were dried in an oven at 105 °C for 24 h, milled and sieved to obtain a uniform particle size, and stored in a desiccator. In this case, the particle size was in the range of 100–150 μm and the initial mass of sample for each run was set to 8 mg to avoid mass and heat transfer limitations.

### 2.2. Experimental procedure

Thermogravimetric analyses (pyrolysis and combustion experiments) were carried out in a TGA apparatus (TGA-DSC 1, METTLER TOLEDO). The biomasses were heated up from ambient temperature to 900 and 1000 for combustion and pyrolysis experiments, respectively, at different heating rates: 5, 10, 15, 20 and 40 °C/min. A volumetric flow of 200 NmL/min of Ar were used for pyrolysis runs whereas a reactive atmosphere of 21 vol.% of oxygen and 79 vol.% of Ar was used for combustion runs. During experiments, the mass loss of the sample and the temperature were recorded. The experimental error of these measurements was calculated, obtaining an error of ±0.5% and ±2 °C in the weight and temperature determination. Further details about the thermogravimetric results of the pyrolysis and combustion experiments can be found in a previous paper (Fernandez-Lopez et al., 2015).

### 2.3. Kinetic methods

Thermogravimetric experiments were carried out with a non-isothermal temperature program. Mass loss was measured as a function of the temperature and time. The rate of the process ($d\alpha/dt$) can be parameterized as a function of the temperature, T; the extent of conversion, α; and the pressure, P as follows:

$$\frac{d\alpha}{dt} = k(T)f(\alpha)h(P) \tag{1}$$

The pressure dependence $h(P)$ is ignored in most of the kinetics studies reported (Vyazovkin et al., 2011). Therefore, the rate is considered to be as a function of the temperature, T, and the extent of conversion, α:

$$\frac{d\alpha}{dt} = k(T)f(\alpha) \tag{2}$$

Eq. (2) represents the reaction rate of a single-step process. Although the process mechanism involves more than one reaction, one of them could determine the overall kinetics (Vyazovkin et al., 2011). Therefore, Eq. (2) can be used to describe the overall reaction rate of the thermochemical processes.

The temperature dependence $k(T)$ is typically parameterized by the Arrhenius equation:

$$k(T) = Ae^{\frac{-E_a}{RT}} \tag{3}$$

where $A$ is the preexponential factor, $E_a$ the activation energy and $R$ the universal gas constant. These kinetic parameters, which are experimentally determined, are called "effective" or "apparent" parameters because represents the overall process and not the individual parameters of each step or reaction. In following sections, the word "apparent" will be omitted but the activation energy will always be referred to the apparent activation energy.

The function which describes the conversion degree can be expressed by using different reaction models, $f(\alpha)$, which are described elsewhere (López-González et al., 2013). The extent of conversion α is defined as follows:

$$\alpha = \frac{m_0 - m_t}{m_0 - m_f} \tag{4}$$

where $m_0$, $m_t$ and $m_f$ represents the mass at time t = 0, t = t and t = $t_f$, respectively.

Combining Eqs. (2) and (3) yields:

$$\frac{d\alpha}{dt} = Ae^{\frac{-E_a}{RT}}f(\alpha) \tag{5}$$

Integrating Eq. (5), the integral function $g(\alpha)$ can be defined as follows:

$$g(\alpha) \equiv \int_0^{\alpha} \frac{d\alpha}{f(\alpha)} = A\int_0^{t} e^{\frac{-E_a}{RT}}dt \tag{6}$$

Defining a constant heating rate as $\beta = dT/dt$, Eq. (6) is rearranged as follows:

$$g(\alpha) \equiv \int_0^{\alpha} \frac{d\alpha}{f(\alpha)} = \frac{A}{\beta}\int_{T_0}^{T} e^{\frac{-E_a}{RT}}dT \tag{7}$$

Eq. (7) is the general equation which is necessary to obtain the kinetic parameters of the biomass thermal decomposition. This equation has not an analytical solution. Therefore, a number of approximate solutions were given in the past (Vyazovkin et al., 2011). There are different methods to solve and obtain the kinetic parameters from Eq. (7). On the one hand, fitting-models allow to

obtain the kinetic parameters by selecting the adequate reaction model $f(\alpha)$ for each biomass decomposition considered during the thermochemical process. In this sense, Eq. (7) is integrated by using the Coats-Redfern method (Coats and Redfern, 1964). In this work, different kinetic models were tested to determine the best linear fit for each stage and once the best fit was obtained, the activation energy was calculated from the slope. On the other hand, iso-conversional methods (model-free methods) are used to obtain these kinetic parameters without the specification of a reaction model. Iso-conversional methods consider that the reaction rate at constant extent of conversion is only function of the temperature. These methods can be split in two categories: differential and integral. In this work, activation energy from dynamic data was obtained from three different iso-conversional methods: Flynn-Wall-Ozawa (FWO) and Kissinger-Akahira-Sunose (KAS) as integral methods; and Friedman as differential method.

Generally, the approximation of iso-conversional methods for Eq. (7) gives rise to linear equations of the general form (Vyazovkin et al., 2011):

$$\ln\left(\frac{\beta_i}{T^B_{\alpha,i}}\right) = Const - C\left(\frac{E_\alpha}{R \cdot T_\alpha}\right) \tag{8}$$

where $\beta_i$ is the heating rate and $T_{\alpha,i}$ is the temperature to reach a given extent of conversion ($\alpha$). $B$ and $C$ are the specific parameters determined by the type of temperature integral approximation. Using these methods, apparent activation energy ($E_a$) is obtained from the slope of the plot of $\ln\left(\frac{\beta_i}{T^B_{\alpha,i}}\right)$ against $1/T_\alpha$, which represents the linear relation of a given value of conversion at different heating rates.

Finally, two different models were applied to predict the weight loss curves of the pyrolysis and combustion processes: the distributed activation energy (DAEM) and the pseudo-multi component stage (PMSM) models. These two models are represented by a set of ordinary equations which is solved by two home-made Excel-Visual Basic applications based on the Runge-Kutta-Fehlberg method for the evaluation of the set of ordinary differential equations raised.

## 3. Results & discussion

As described in the previous work (Fernandez-Lopez et al., 2015), the derivate thermogravimetric (DTG) profile of the swine (SW) and dairy (Pre and Dig R) manure samples pyrolysis showed one main decomposition which was related to the devolatilization stage. The difference between swine and dairy samples was the number of peaks which describes the devolatilization stage, being one for Pre and Dig R samples and two for SW sample. This difference was attributed to the composition of the samples. On the other hand, the combustion of these samples showed two main decomposition peaks: devolatilization (as pyrolysis) and char oxidation. In the following sections, the study of the kinetics of the different pyrolysis and combustion stages was carried out according to different methods described in the previous section (Section 2.3).

### 3.1. Model-fitting method: Coats-Redfern

Using the model-fitting Coats-Redfern, Eq. (7) can be integrated as follows:

$$\ln\left[\frac{g(\alpha)}{T^2}\right] = \ln\left[\frac{A \cdot R}{\beta \cdot E_a \cdot \left(1 - \frac{2 \cdot R \cdot T}{E_a}\right)}\right]^{\frac{-E_a}{R \cdot T}} \tag{9}$$

If the correct expression of $g(\alpha)$ is used, the plot of $\ln\left[\frac{g(\alpha)}{T^2}\right]$ against $1/T$ should give a straight line with a high correlation coefficient of the linear regression analysis, from which the values of $E_a$ and $A$ can be easily calculated from the slope and the intercept term, respectively. The term $\frac{2 \cdot R \cdot T}{E_a}$ can be neglected as it is less than the unit. Therefore, the intercept can be arranged as $\ln\left(\frac{A \cdot R}{\beta \cdot E_a}\right)$ where $A$ can be calculated (López-González et al., 2013; Garcia-Maraver et al., 2015). The functions $f(\alpha)$ and $g(\alpha)$ referred to the different reaction models and its integrated form, respectively, are shown in Table 1 (White et al., 2011).

Using the Coats-Redfern method, activation energy ($E_a$) for each thermochemical process stage can be calculated. Figs. SS1 and SS2

**Table 1**
Expressions for the reaction mechanisms and its integrated form in solid state reactions.

| Reaction model | $f(\alpha)$ | $g(\alpha)$ | Hypothesis (Brown, 1998) |
|---|---|---|---|
| *Reaction order* | | | |
| $O_0$ | $(1-\alpha)^n$ | $\alpha$ | The decomposition of particles occurs by following a random nucleation and growth does not advance beyond the individual crystallite nucleated |
| $O_1$ | | $-\ln(1-\alpha)$ | |
| $O_2$ | | $-(1-\alpha)^{-1}$ | |
| $O_3$ | | $1/2\ (1-\alpha)^{-2}$ | |
| *Phase boundary controlled reaction* | | | |
| $R_2$ | $(1-\alpha)^{(1-1/n)}$ | $1-(1-\alpha)^{(1/2)}$ | Contracting geometry models are based on an initial rapid dense nucleation across crystal faces. Close spacing results in the rapid generation of a reaction zone that advances at a constant rate without diffusion effects |
| $R_3$ | | $1-(1-\alpha)^{(1/3)}$ | |
| *Power law* | | | |
| $P_1$ | $n(\alpha)^{(1-1/n)}$ | $\alpha^{1/4}$ | The power law of nucleation is based on the acceleratory nucleation process and several distinct steps are required to generate a growth nucleus |
| $P_2$ | | $\alpha^{1/3}$ | |
| $P_3$ | | $\alpha^{1/2}$ | |
| $P_4$ | | $\alpha^{3/2}$ | |
| *Nucleation and growth (Avrami-Erofeev equation)* | | | |
| $N_1$ | $n(1-\alpha)[-\ln(1-\alpha)]^{(1-1/n)}$ | $[-\ln(1-\alpha)]^{(1/1.5)}$ | This model is also based on the acceleratory nucleation process but the number of dimensions in which nuclei growth is also taking into account |
| $N_2$ | | $[-\ln(1-\alpha)]^{(1/2)}$ | |
| $N_3$ | | $[-\ln(1-\alpha)]^{(1/3)}$ | |
| $N_4$ | | $[-\ln(1-\alpha)]^{(1/4)}$ | |
| *Diffusion* | | | |
| $D_1$ | $1/2\alpha$ | $\alpha^2$ | Diffusion models are based on reaction at which the transport of reactants or products from the site of chemical change may be controlled by a diffusion process if this transport is slower than the chemical steps |
| $D_2$ | $[-\ln(1-\alpha)]^{-1}$ | $(1-\alpha)\ln(1-\alpha)+\alpha$ | |
| $D_3$ | $3/2(1-\alpha)^{2/3}[1-(1-\alpha)^{1/3}]^{-1}$ | $[1-(1-\alpha)^{1/3}]^2$ | |
| $D_4$ | $3/2[(1-\alpha)^{1/3}-1]^{-1}$ | $1-2/3\alpha-(1-\alpha)^{2/3}$ | |

**Table 2**
Activation energies obtained from Coats-Redfem method for the pyrolysis of the three manure samples.

| Sample | Heating rate (°C/min) | $r^2$ | Ea (kJ/mol) | $r^2$ | Ea (kJ/mol) | $r^2$ | Ea (kJ/mol) |
|---|---|---|---|---|---|---|---|
| Pre | *Pyrolysis Devolatilization ($D_3$)* | | | *Combustion Devolatilization ($D_3$)* | | *Char oxidation ($O_{3.75}$)* | |
| | 5 | 0.967 | 147 | 0.996 | 137 | 0.965 | 156 |
| | 10 | 0.976 | 144 | 0.996 | 143 | 0.971 | 164 |
| | 15 | 0.962 | 156 | 0.988 | 152 | 0.950 | 175 |
| | 20 | 0.986 | 149 | 0.999 | 148 | 0.937 | 177 |
| | 40 | 0.965 | 164 | 0.988 | 162 | 0.950 | 183 |
| Dig R | *Pyrolysis Devolatilization ($D_3$)* | | | *Combustion Devolatilization ($D_3$)* | | *Char oxidation ($O_3$)* | |
| | 5 | 0.969 | 141 | 1.000 | 138 | 0.951 | 171 |
| | 10 | 0.977 | 137 | 0.999 | 142 | 0.941 | 170 |
| | 15 | 0.972 | 147 | 0.998 | 146 | 0.937 | 172 |
| | 20 | 0.973 | 150 | 0.999 | 147 | 0.934 | 187 |
| | 40 | 0.956 | 165 | 0.999 | 146 | 0.939 | 188 |
| SW | *Pyrolysis Devolatilization ($D_3$)* | | | *Combustion Devolatilization ($D_3$)* | | *Char oxidation ($O_2$)* | |
| | 5 | 0.973 | 144 | 0.988 | 181 | 0.956 | 126 |
| | 10 | 0.965 | 145 | 0.983 | 177 | 0.914 | 123 |
| | 15 | 0.977 | 155 | 0.991 | 193 | 0.890 | 121 |
| | 20 | 0.986 | 165 | 0.987 | 186 | 0.869 | 121 |
| | 40 | 0.978 | 168 | 0.98 | 190 | 0.865 | 119 |

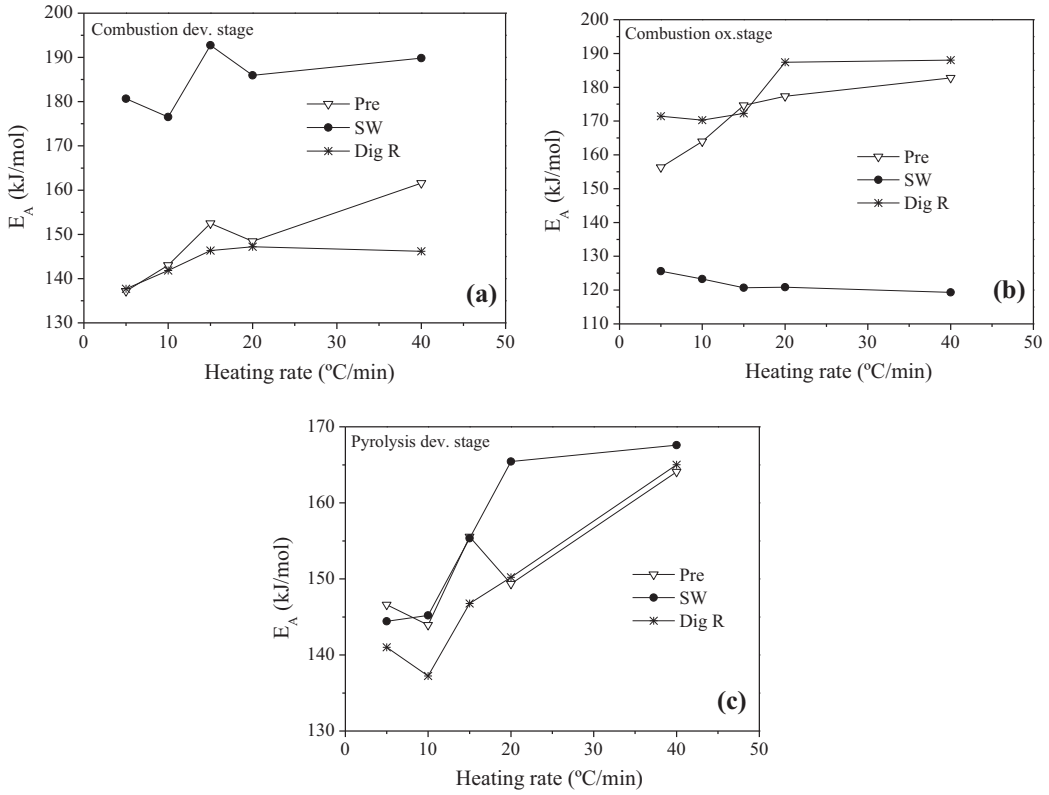


**Fig. 1.** Comparison of the activation energy for: (a) combustion devolatilization, (b) char oxidation and (c) pyrolysis devolatilization.

shows the linear plot of $\ln\left[\frac{g(\alpha)}{T^2}\right]$ against $1/T$ for the pyrolysis and combustion processes, respectively, of samples SW, Pre and Dig R at different heating rates. It is important to highlight that different kinetic models were tested to determine the best linear fit for each stage. Once the best fit was obtained, the activation energy was calculated from the slope as described in Section 2. Table 2 shows the activation energies calculated for the devolatilization stage of pyrolysis for the three samples studied at different heating rates. Furthermore, the best kinetic model for each sample is also shown as well as the correlation coefficient. The same values for the combustion process are also shown in Table 2.

It was observed from Table 2 that diffusional models (Table 1) were the best models which describe the kinetic of the devolatilization stage in both pyrolysis and combustion process. Among the different diffusional models, the best linear fit was obtained with the diffusional model 3 ($D_3$). The average value of the activation energy of the pyrolysis devolatilization stage for samples SW, Pre and Dig R were 156, 152 and 148 kJ/mol, respectively. Regarding the combustion process, similar values were found for the devolatilization stage, being 185, 149 and 144 kJ/mol for samples SW, Pre and Dig R, respectively. Generally, both devolatilization stages show similar activation energy values except for sample SW.

Concerning the char oxidation stage in combustion experiments, the best correlation coefficients were obtained using *n*-order kinetic models. Several orders were tested for each sample, concluding that order 2, 3 and 3.75 were the best for samples SW, Dig R and Pre, respectively. Activation energies of the char oxidation stages calculated for dairy samples were higher than those of the devolatilization stages except for sample SW. In this sense, activation energies of the char oxidation stages were 171, 178 and 122 kJ/mol for samples Pre, Dig R and SW, respectively.

Generally speaking, Table 2 shows that the heating rate did not considerably affect the activation energy and there were no significant differences among the values obtained (see Fig. 1).

### 3.2. Model-free methods: Flynn-Wall-Ozawa (FWO), Kissinger-Akahira-Sunose (KAS) and Friedman

Activation energies ($E_a$) of the thermochemical processes studied were also obtained using model-free methods. The differences among them are the approximation used to solve Eq. (8). One of these approximations is that of Doyle (1962) so that Eq. (8) takes the form also known as the Flynn-Wall-Ozawa (FWO) equation:

$$\ln(\beta_i) = Const - 1.052\left(\frac{E_\alpha}{R \cdot T_\alpha}\right) \quad (10)$$

On the other hand, KAS method (Vyazovkin et al., 2011; Slopiecka et al., 2012) is based on the following expression:

$$\ln\left(\frac{\beta_i}{T_{\alpha,i}^2}\right) = Const - \left(\frac{E_\alpha}{R \cdot T_\alpha}\right) \quad (11)$$

Finally, the Friedman method (Friedman, 1969) is the most common differential iso-conversional method and is based on the following equation:

$$\ln\left[\beta_i\left(\frac{d\alpha}{dT}\right)_{\alpha,i}\right] = \ln[f(\alpha) \cdot A_\alpha] - \frac{E_\alpha}{R \cdot T_{\alpha,i}} \quad (12)$$

As aforementioned, these are linear equations and the activation energy at a given extent of conversion can be calculated from the slope when *the first term* is represented against $1/T_{\alpha,i}$.

According to Eqs. (10)–(12) the activation energy of the pyrolysis and combustion of the three samples studied were calculated by using FWO, KAS and Friedman methods, respectively, for a given extent of conversion ($\alpha$). Regarding the Coats-Redfern method, the activation energy was obtained from the slope of a linear representation of the experimental data according to the previous cited equations.

Fig. SS3 shows the linear representation for the experiments of pyrolysis based on FWO, KAS and Friedman methods at different extent of conversion. Activation energies and correlation coefficients ($r^2$) calculated from these representations are shown in Table 3. The temperature range, which corresponds to the extent of conversion range selected, is also shown. Taking into account that the main stage during the pyrolysis of the samples was included, the initial and final extents of conversion selected were the ones with the highest correlation coefficient.

As Table 3 shows, in some cases, the linear plots presented high correlation coefficients in the range of 0.915–1.000.

Fig. 2 represents the activation energy values against conversion for the pyrolysis of the three biomass samples obtained by iso-conversional methods. The three methods presented the same trend and the values obtained of activation energy were similar (Xiao et al., 2009). The activation energy values obtained by the Friedman method (integral one) presented some variation if compared to FWO and KAS, being those obtained with the former higher than those obtained with the latter (Vyazovkin et al., 2011). Furthermore, there was an increase in the activation energy with the extent of conversion, which indicated that the pyrolysis process is kinetically complex and the reaction mechanism changed during the process (Vyazovkin et al., 2011; Papari and Hawboldt, 2015). However, the activation energy could be considered to be constant in the main region of the pyrolysis (devolatilization) process.

Regarding the combustion process, the same procedure was used to calculate activation energy values. The linear representation of experimental data based on FWO, KAS and Friedman methods at different extent of conversion for combustion experiments is shown in Fig. SS4. Furthermore, activation energies and correlation coefficients ($r^2$) obtained from these plots are shown in Table 4. Activation energy values are also represented against conversion in Fig. 2.

In this case, two regions of activation energy can be observed, corresponding to the two main stages of the combustion process: devolatilization and char oxidation.

Generally speaking, Fig. 2 shows that the activation energy of the devolatilization stage for the three samples reached a constant value in the range of 0.05 and 0.5 of extent of conversion. These values of activation energy were lower for dairy samples than that obtained for the pyrolysis process. However, the activation energy value for sample SW was the same as that obtained in combustion experiments (≈200 kJ/mol). Respecting the char oxidation stage, activation energy values were calculated in the extent of conversion ranging from 0.6 to 0.9. The values of the char oxidation stage for dairy samples were higher than that obtained for the devolatilization stage. In the case of sample SW, the lower activation energy was obtained for this stage. Furthermore, sample Pre showed a continuous increase of the activation energy which would indicate that the mechanism of decomposition changed with the extent of conversion.

To sum up, the average activation energy obtained for the pyrolysis and combustion of samples Pre, Dig R and SW are shown in Table 5. The conversion and the temperature range considered for the calculation of the activation energy are also shown.

The activation energy values obtained by different iso-conversional methods were very similar (Table 5). In the case of dairy samples (Pre and Dig R), the values of the activation energy were almost the same regardless the method used, pointing out that the kinetic mechanism which took place during the decomposition of the manure samples was not affected by the anaerobic digestion.

On the other hand, the values of the activation energy calculated by the Coats-Redfem method for both stages of the combustion process were very similar to that obtained by iso-conversional methods. In the case of the pyrolysis process, the activation energy values obtained for the devolatilization stage by the Coats-Redfern method were lower than those obtained by the iso-conversional methods. The maximum difference among the different activation energy values was about 53 kJ/mol. Therefore, there was no significant difference in value when the Coats-Redfern and iso-conversional methods were used to calculate the values of the activation energy. However, if the pre-exponential factor has to be calculated, Coats-Redfern method has to be used because iso-conversional methods do not consider it (Ceylan and Topçu, 2014).

### 3.3. Prediction of the weight loss curves

It is assumed in the distributed activation energy model (DAEM) that the mechanism of biomass thermal decomposition can be defined by a multiple parallel and independent *n*-order reactions. Each reaction can be described by an activation energy distribution focused on a medium value with a temperature range which covers this value depending on the standard deviation. The global thermal decomposition reflects the sum of each thermal

**Table 3**
Activation energies and correlation coefficients calculated by iso-conversional methods for the pyrolysis of the three biomass samples studied.

| Sample Pre (Temperature range 170–360 °C) | | | | | | | Sample Dig R (Temperature range 180–355 °C) | | | | | | Sample SW (Temperature range 180–350 °C) | | | | | |
|---|---|---|---|---|---|---|---|---|---|---|---|---|---|---|---|---|---|---|
| | Friedman | | FWO | | KAS | | Friedman | | FWO | | KAS | | Friedman | | FWO | | KAS | |
| Conversion (α) | $r^2$ | Ea (kJ/mol) | $r^2$ | Ea (kJ/mol) | $r^2$ | Ea (kJ/mol) | $r^2$ | Ea (kJ/mol) | $r^2$ | Ea (kJ/mol) | $r^2$ | Ea (kJ/mol) | $r^2$ | Ea (kJ/mol) | $r^2$ | Ea (kJ/mol) | $r^2$ | Ea (kJ/mol) |
| 0.01 | 0.964 | 118 | 0.977 | 125 | 0.973 | 111 | 0.915 | 95 | 0.953 | 115 | 0.946 | 102 | 0.960 | 113 | 0.970 | 125 | 0.965 | 111 |
| 0.03 | 0.986 | 133 | 0.984 | 141 | 0.982 | 126 | 0.998 | 128 | 0.981 | 143 | 0.978 | 127 | 0.999 | 142 | 0.994 | 152 | 0.993 | 136 |
| 0.05 | 0.990 | 143 | 0.988 | 152 | 0.986 | 136 | 0.993 | 141 | 0.985 | 153 | 0.983 | 137 | 0.994 | 157 | 0.997 | 160 | 0.997 | 144 |
| 0.07 | 0.991 | 146 | 0.989 | 155 | 0.987 | 139 | 0.992 | 152 | 0.989 | 162 | 0.988 | 146 | 0.994 | 154 | 0.998 | 166 | 0.998 | 149 |
| 0.09 | 0.993 | 152 | 0.992 | 161 | 0.991 | 144 | 0.987 | 158 | 0.990 | 165 | 0.989 | 148 | 0.994 | 162 | 0.997 | 169 | 0.997 | 152 |
| 0.11 | 0.990 | 153 | 0.993 | 164 | 0.992 | 147 | 0.992 | 166 | 0.990 | 171 | 0.989 | 153 | 0.996 | 169 | 0.998 | 173 | 0.998 | 155 |
| 0.15 | 0.992 | 161 | 0.993 | 171 | 0.992 | 153 | 0.992 | 176 | 0.991 | 180 | 0.990 | 162 | 0.994 | 173 | 0.996 | 178 | 0.995 | 160 |
| 0.19 | 0.992 | 168 | 0.992 | 175 | 0.991 | 157 | 0.995 | 181 | 0.993 | 189 | 0.992 | 170 | 0.995 | 187 | 0.997 | 187 | 0.996 | 169 |
| 0.23 | 0.991 | 176 | 0.993 | 182 | 0.992 | 164 | 0.990 | 197 | 0.993 | 200 | 0.992 | 181 | 0.993 | 199 | 0.996 | 196 | 0.995 | 177 |
| 0.27 | 0.987 | 189 | 0.991 | 191 | 0.990 | 172 | 0.993 | 204 | 0.991 | 207 | 0.990 | 187 | 0.988 | 210 | 0.993 | 202 | 0.992 | 183 |
| 0.31 | 0.989 | 191 | 0.989 | 195 | 0.988 | 176 | 0.990 | 218 | 0.991 | 217 | 0.990 | 196 | 0.988 | 231 | 0.992 | 217 | 0.992 | 197 |
| 0.35 | 0.987 | 200 | 0.988 | 202 | 0.987 | 182 | 0.982 | 241 | 0.987 | 231 | 0.985 | 210 | 0.981 | 247 | 0.986 | 229 | 0.985 | 209 |
| 0.39 | 0.984 | 215 | 0.989 | 214 | 0.988 | 194 | 0.975 | 282 | 0.979 | 258 | 0.978 | 235 | 0.988 | 258 | 0.985 | 251 | 0.983 | 229 |
| 0.43 | 0.975 | 228 | 0.983 | 221 | 0.981 | 200 | 0.951 | 367 | 0.959 | 311 | 0.956 | 286 | 0.990 | 255 | 0.982 | 263 | 0.981 | 241 |
| 0.47 | 0.962 | 242 | 0.974 | 238 | 0.971 | 216 | 0.915 | 423 | 0.928 | 386 | 0.924 | 357 | 0.990 | 253 | 0.986 | 271 | 0.985 | 248 |
| 0.51 | 0.936 | 301 | 0.957 | 271 | 0.953 | 247 | – | – | – | – | – | – | 0.997 | 239 | 0.993 | 275 | 0.993 | 251 |
| 0.55 | – | – | 0.907 | 310 | 0.901 | 284 | – | – | – | – | – | – | 0.995 | 242 | 0.992 | 268 | 0.991 | 245 |
| 0.59 | – | – | – | – | – | – | – | – | – | – | – | – | 0.989 | 268 | 0.993 | 275 | 0.993 | 251 |
| 0.63 | – | – | – | – | – | – | – | – | – | – | – | – | 0.944 | 335 | 0.980 | 290 | 0.978 | 265 |

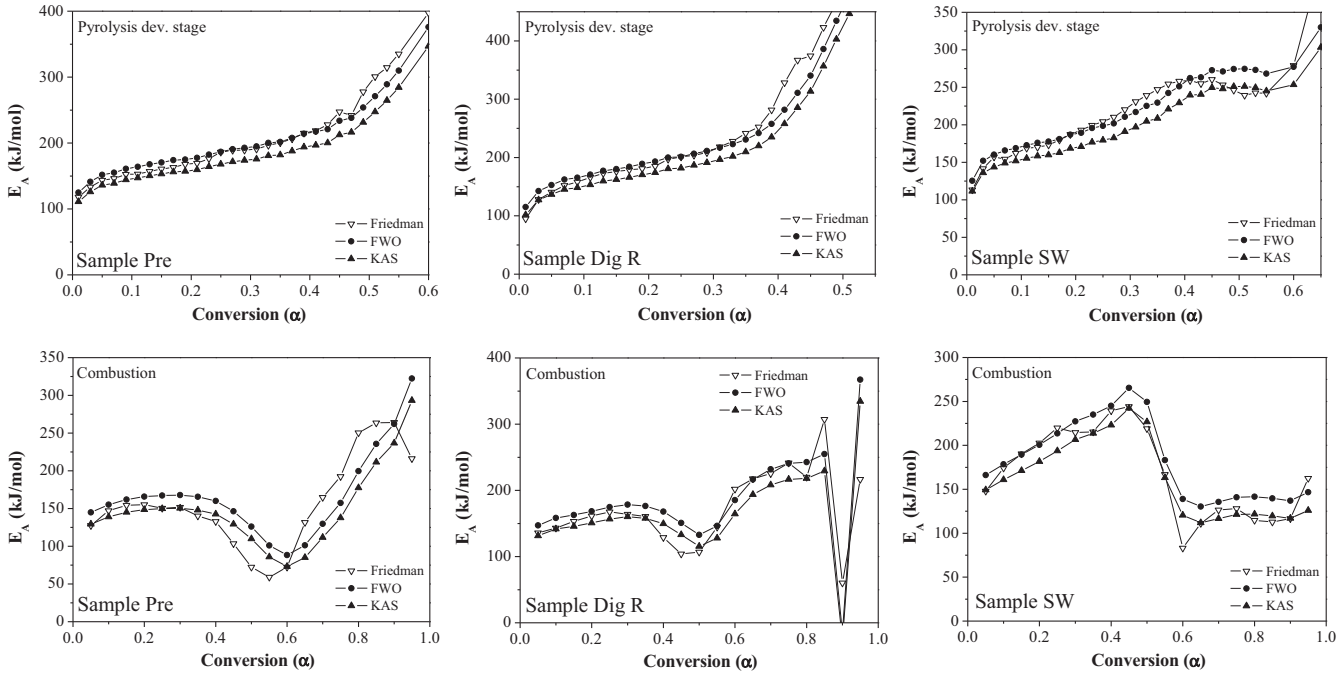


**Fig. 2.** Activation energy vs extent of conversion for the combustion process of the three manure biomass studied.

decomposition behavior, weighted by the composition of the biomass studied (Várhegyi et al., 2011; Cai et al., 2013).

The general equation of this model for an *n*-order reaction and one decomposition stage is given below:

$$\frac{da}{dt} = \int_0^{\infty} A\exp\left(-\frac{E_a}{RT}\right)\left[1-(1-n)\int_0^t A\exp\left(-\frac{E_a}{RT}\right)dt\right]^{\frac{n}{1-n}} f(E_a)dE_a \tag{13}$$

where $A$, $E_a$, $R$ and $f(E)$ are the preexponential factor, activation energy, universal gas constant and distribution function of activation energy, respectively (Cai et al., 2014).

Several forms of $f(E)$ have been reported in literature (Cai et al., 2014). One of the most used is the Gaussian distribution (de Caprariis et al., 2012) centered at $E_0$ with standard deviation $\sigma$:

$$f(E_a) = \frac{1}{\sigma\sqrt{2\pi}}\exp\left[-\frac{(E_a-E_0)^2}{2\sigma^2}\right] \tag{14}$$

where $E_0$ is the mean value of the activation energy distribution and $\sigma$ is the standard deviation of the activation energy distribution.

Taking into account the heating rate $\beta$, Eq. (13) is rearranged as:

$$\frac{da}{dT} = \sum_{i=1}^{m} c_i \int_0^{\infty} \frac{A_{0,i}}{\beta}\exp\left(-\frac{E_a}{RT}\right)\left[1-(1-n)\int_{T_0}^{T}\exp\frac{A_{0,i}}{\beta}\left(-\frac{E_a}{RT}\right)dT\right]^{n/(1-n)} f(E)dE_a \tag{15}$$

where $c_i$ is the fraction of volatiles produced by each $i_{th}$ decomposition stage, $m$ is the number of fitted peak which corresponds to each decomposition stage (Zhang et al., 2015) and $n$ is the reaction order.

As there is no analytical solution to Eq. (15) and due to its mathematical complexity, a home-made Excel Visual Basic application (VBA) was developed. This application was used to evaluate the integral terms by the Simpson method and to solve the non-linear equation system generated by the Marquardt algorithm (Sun et al., 2015). The unknown parameters $c_i$, $A_{o,i}$, $\sigma_i$, $E_a$ and $E_{o,i}$, were calculated by evaluating the derivative thermogravimetric (DTG) obtained experimentally. Moreover, in good agreement with other authors (Damartzis et al., 2011; Cai et al., 2013; Sharara et al., 2014; Zhang et al., 2015), the objective function (O.F.) and Fit parameter were based on the DTG data to optimize these unknown parameters and defined by the following equations:

$$O.F. = \sum_{i=1}^{n_d}\left[\left(\frac{d\alpha}{dT}\right)_{exp,i} - \left(\frac{d\alpha}{dT}\right)_{cal,i}\right]^2 \tag{16}$$

$$Fit(\%) = 100\cdot\frac{\sqrt{O.F./n_d}}{\left(\frac{d\alpha}{dT}\right)_{max}} \tag{17}$$

Other authors studied the kinetic decomposition of different biomass using the DAEM model (Navarro et al., 2008; Chen et al., 2011; Kirtania and Bhattacharya, 2012; Várhegyi et al., 2012; Cai et al., 2013; Tran et al., 2014).

On the other hand, in the PMSM model, it is supposed that separated reactions corresponding to each thermal decomposition stage take place. This way, the overall process will be described considering $n$ separate reactions (one for each decomposition stage). The kinetic rate of biomass thermal decomposition can be derived from Eq. (17):

$$\frac{d\alpha_i}{dT} = \frac{A_i}{\beta}\cdot e^{\frac{E_{a,i}}{RT}}\cdot f_i(\alpha_i) \tag{17}$$

where $\alpha_i$, $A_i$, $E_{a,i}$ and $f_i(\alpha_i)$ are the degree of conversion, the pre-exponential factor, the activation energy and the model functions obtained for each stage of the pyrolysis and combustion processes, respectively. The set of ordinary equations will be solved by the home-made Excel Visual Basic application developed and based on the Runge-Kutta-Fehlberg method.

Regarding the results of the pyrolysis experiments obtained by using the Coats-Redfern method in the previous subsection, the best model ($f(\alpha)$) which described the devolatilization stage of the three samples studied was the diffusional model 3 ($D_3$). Therefore, model $D_3$ was used in the case of PMSM model for the reconstruction of the weight loss curves. Concerning the char oxidation stage of combustion process, $n$-order kinetic models were selected as the best ones for this stage and, therefore, substituted in Eq. (17) for the curves reconstruction. Figs. 3 and 4 show the reconstruction

**Table 4**
Activation energies and correlation coefficients calculated by iso-conversional methods for the combustion of the three biomass samples studied.

| Sample Pre (Temperature range 220–530 °C) | | | | | | | Sample Dig R (Temperature range 225–630 °C) | | | | | | Sample SW (Temperature range 230–590 °C) | | | | | |
|---|---|---|---|---|---|---|---|---|---|---|---|---|---|---|---|---|---|---|
| | Friedman | | FWO | | KAS | | Friedman | | FWO | | KAS | | Friedman | | FWO | | KAS | |
| Conversión (α) | $r^2$ | Ea (kJ/mol) | $r^2$ | Ea (kJ/mol) | $r^2$ | Ea (kJ/mol) | $r^2$ | Ea (kJ/mol) | $r^2$ | Ea (kJ/mol) | $r^2$ | Ea (kJ/mol) | $r^2$ | Ea (kJ/mol) | $r^2$ | Ea (kJ/mol) | $r^2$ | Ea (kJ/mol) |
| 0.05 | 0.996 | 127 | 0.996 | 145 | 0.996 | 129 | 0.999 | 136 | 0.995 | 147 | 0.995 | 131 | 0.999 | 148 | 0.999 | 166 | 0.999 | 149 |
| 0.1 | 0.999 | 147 | 0.998 | 155 | 0.997 | 139 | 0.996 | 143 | 0.996 | 158 | 0.995 | 142 | 0.999 | 174 | 1.000 | 179 | 1.000 | 161 |
| 0.15 | 0.998 | 154 | 0.999 | 162 | 0.998 | 145 | 0.992 | 153 | 0.995 | 163 | 0.994 | 146 | 0.999 | 190 | 0.999 | 190 | 0.999 | 171 |
| 0.2 | 0.996 | 155 | 0.998 | 166 | 0.997 | 149 | 0.986 | 161 | 0.992 | 168 | 0.991 | 151 | 0.999 | 203 | 1.000 | 201 | 1.000 | 182 |
| 0.25 | 0.993 | 151 | 0.997 | 167 | 0.997 | 150 | 0.981 | 167 | 0.988 | 175 | 0.987 | 157 | 0.999 | 220 | 0.999 | 214 | 0.999 | 194 |
| 0.3 | 0.990 | 152 | 0.995 | 168 | 0.994 | 150 | 0.968 | 164 | 0.984 | 178 | 0.982 | 160 | 0.992 | 215 | 0.998 | 227 | 0.998 | 207 |
| 0.35 | 0.981 | 140 | 0.992 | 166 | 0.992 | 148 | 0.954 | 161 | 0.975 | 176 | 0.971 | 158 | 0.987 | 215 | 0.994 | 235 | 0.994 | 214 |
| 0.4 | 0.971 | 133 | 0.987 | 160 | 0.985 | 143 | 0.939 | 129 | 0.967 | 168 | 0.962 | 150 | 0.989 | 239 | 0.99 | 245 | 0.989 | 223 |
| 0.45 | 0.956 | 104 | 0.983 | 146 | 0.981 | 129 | 0.884 | 104 | 0.954 | 151 | 0.947 | 133 | 0.959 | 244 | 0.986 | 265 | 0.985 | 242 |
| 0.5 | 0.916 | 72 | 0.979 | 126 | 0.976 | 110 | 0.947 | 107 | 0.937 | 133 | 0.926 | 115 | 0.843 | 219 | 0.935 | 249 | 0.929 | 227 |
| 0.55 | 0.863 | 59 | 0.974 | 101 | 0.968 | 86 | 0.951 | 144 | 0.947 | 146 | 0.938 | 128 | 0.94 | 167 | 0.901 | 183 | 0.889 | 163 |
| 0.6 | 0.970 | 72 | 0.965 | 88 | 0.955 | 73 | 0.975 | 202 | 0.958 | 185 | 0.952 | 164 | 0.839 | 83 | 0.95 | 139 | 0.941 | 120 |
| 0.65 | 0.966 | 132 | 0.950 | 101 | 0.937 | 85 | 0.956 | 218 | 0.959 | 216 | 0.954 | 194 | 0.898 | 111 | 0.944 | 130 | 0.932 | 112 |
| 0.7 | 0.971 | 165 | 0.941 | 130 | 0.929 | 112 | 0.956 | 225 | 0.955 | 232 | 0.950 | 208 | 0.989 | 126 | 0.954 | 136 | 0.944 | 117 |
| 0.75 | 0.974 | 192 | 0.940 | 157 | 0.930 | 138 | 0.931 | 241 | 0.957 | 241 | 0.952 | 217 | 0.994 | 128 | 0.976 | 141 | 0.972 | 121 |
| 0.8 | 0.993 | 250 | 0.956 | 200 | 0.950 | 177 | 0.928 | 220 | 0.954 | 243 | 0.948 | 218 | 0.989 | 115 | 0.991 | 142 | 0.99 | 122 |
| 0.85 | 0.983 | 264 | 0.964 | 236 | 0.960 | 212 | – | – | 0.931 | 255 | 0.924 | 229 | 0.988 | 113 | 0.997 | 140 | 0.996 | 120 |
| 0.9 | 0.900 | 264 | 0.962 | 262 | 0.958 | 237 | – | – | – | – | – | – | 0.985 | 117 | 0.998 | 137 | 0.997 | 117 |
| 0.95 | – | – | – | – | – | – | – | – | – | – | – | – | 0.979 | 162 | 0.997 | 147 | 0.996 | 126 |

**Table 5**
Comparison between activation energy values obtained by iso-conversional methods and Coats-Redfern method for all the samples and for both pyrolysis and combustion processes.

| Sample | Stage | Ea (kJ/mol) | | | |
|---|---|---|---|---|---|
| | | Friedman | FWO | KAS | Coats-Redfem |
| Pre | Devolatilization Pyrolysis | 170 | 175 | 157 | 152 |
| Dig R | | 171 | 178 | 160 | 148 |
| SW | | 203 | 209 | 189 | 156 |
| Pre | Devolatilization Combustion | 127 | 152 | 134 | 149 |
| Dig R | | 143 | 162 | 144 | 144 |
| SW | | 200 | 207 | 187 | 185 |
| Pre | Char oxidation Combustion | 175 | 159 | 140 | 171 |
| Dig R | | 194 | 199 | 178 | 178 |
| SW | | 125 | 144 | 124 | 122 |

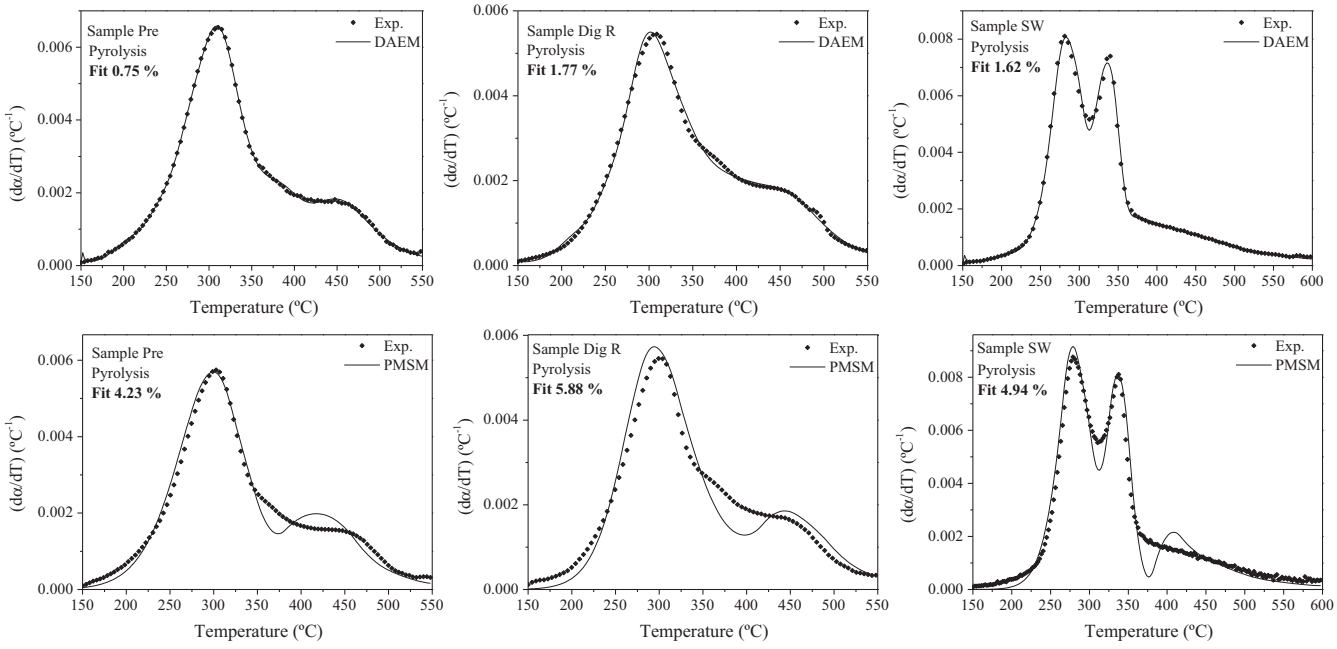


**Fig. 3.** Predicted and experimental DTG curves of manure samples pyrolysis at 15 °C/min using models DAEM and PMSM.

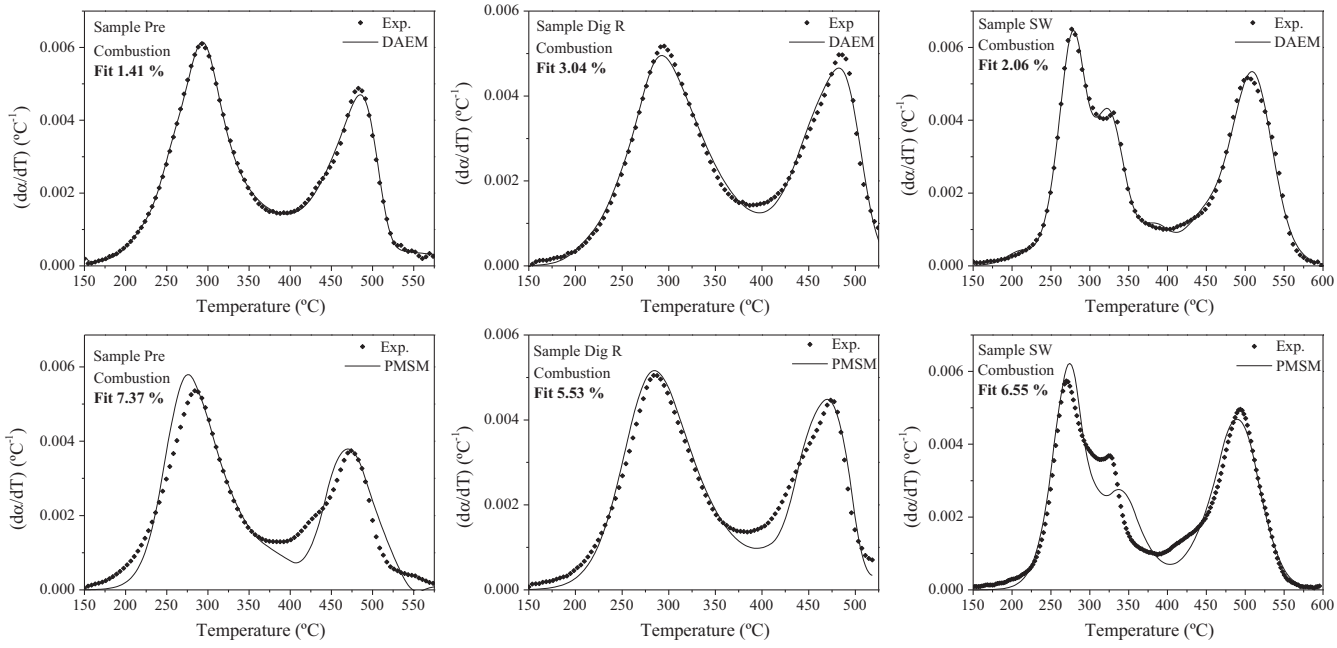


**Fig. 4.** Predicted and experimental DTG curves of manure samples combustion at 15 °C/min using models DAEM and PMSM.

**Table 6**
Kinetic parameters obtained by model DAEM.

| Sample | Pre | | Dig R | | SW | |
|---|---|---|---|---|---|---|
| Process | Pyrolysis | Combustion | Pyrolysis | Combustion | Pyrolysis | Combustion |
| $n_1$ | 2.37 | 1.00 | 2.44 | 3.85 | 1.01 | 1.27 |
| $A_{0,1}$ ($s^{-1}$) | 1.572E+14 | 3.417E+12 | 7.720E+10 | 3.272E+14 | 3.069E+15 | 1.550E+11 |
| $E_{0,1}$ (kJ/mol) | 185 | 208 | 179 | 177 | 195 | 208 |
| $\sigma_1$ (kJ/mol) | 12 | 3 | 3 | 10 | 5 | 4 |
| $c_1$ | 0.57 | 0.25 | 0.39 | 0.39 | 0.65 | 0.33 |
| $n_2$ | 2.69 | 10.00 | 3.00 | 1.17 | 3.47 | 1.00 |
| $A_{0,2}$ ($s^{-1}$) | 3.526E+12 | 2.263E+15 | 3.899E+13 | 3.243E+13 | 6.733E+17 | 4.525E+12 |
| $E_{0,2}$ (kJ/mol) | 211 | 193 | 172 | 221 | 224 | 189 |
| $\sigma_2$ (kJ/mol) | 3 | 20 | 13 | 2 | 32 | 24 |
| $c_2$ | 0.22 | 0.53 | 0.61 | 0.69 | 0.35 | 0.30 |
| $n_3$ | 2.57 | 2.12 | | | | 3.53 |
| $A_{0,3}$ ($s^{-1}$) | 9.303E+12 | 2.230E+15 | | | | 1.180E+15 |
| $E_{0,3}$ (kJ/mol) | 154 | 183 | | | | 194 |
| $\sigma_3$ (kJ/mol) | 12 | 9 | | | | 10 |
| $c_3$ | 0.21 | 0.23 | | | | 0.37 |

**Table 7**
Kinetic parameters obtained by model PMSM.

| Sample | Pre | | Dig R | | SW | |
|---|---|---|---|---|---|---|
| Process | Pyrolysis | Combustion | Pyrolysis | Combustion | Pyrolysis | Combustion |
| $n_1$ | 1.26 | 3.51 | 2.37 | 2.63 | 1.08 | 1.52 |
| $A_1$ ($s^{-1}$) | 4.453E+07 | 3.773E+13 | 1.509E+10 | 2.237E+09 | 1.824E+13 | 5.390E+14 |
| $E_{a,1}$ (kJ/mol) | 78 | 130 | 104 | 81 | 118 | 135 |
| $n_2$ | 2.35 | – | 2.82 | – | 0.93 | 2.30 |
| $A_2$ ($s^{-1}$) | 1.373E+12 | 3.996E+12 | 7.412E+14 | 9.972E+13 | 6.323E+15 | 3.029E+14 |
| $E_{a,2}$ (kJ/mol) | 153 | 169 | 196 | 170 | 158 | 150 |
| $n_3$ | | | | | | – |
| $A_3$ ($s^{-1}$) | | | | | | 1.347E+13 |
| $E_{a,3}$ (kJ/mol) | | | | | | 173 |

of the pyrolysis and combustion weight loss curves (DTG curves), respectively, of the three samples by using both PMSM and DAEM models at 15 °C/min. The reconstruction of the rest of the pyrolysis and combustion curves at 5, 10, 20 and 40 °C/min presented similar results. Predicted data (solid line) reproduced the experimental values (dotted line) satisfactorily. Relating to the fit parameter defined in the methodology section and shown in Figs. 3 and 4, the lower the value of this parameter, the better the fitting process is. Therefore, model DAEM fitted better the experimental than model PMSM. Finally, the unknown parameters $n_i$, $c_i$, $A_{o,i}$, $\sigma_i$, $E_a$ and $E_{o,i}$; and $n_i$, $A_i$ and $E_a$; obtained by models DAEM and PSMS, respectively, are shown in Tables 6 and 7.

## 4. Conclusions

The kinetic analysis showed that the activation energy ($E_a$) values of pyrolysis devolatilization stages were in the range of 152–170 kJ/mol, 148–178 kJ/mol and 156–209 kJ/mol for samples Pre, Dig R and SW, respectively. Regarding combustion process, $E_a$ of devolatilization stage was between 127 and 149 kJ/mol, 143 and 162 kJ/mol and 185 and 207 kJ/mol for samples Pre, Dig R and SW, respectively. Char oxidation stages showed lower $E_a$ values than that obtained for the combustion devolatilization stage, being in the range of 140–175 kJ/mol, 178–199 kJ/mol and 122–144 kJ/mol for samples Pre, Dig R and SW, respectively. $E_a$ values obtained from all the methods were practically the same for samples Pre and Dig R, which means that the kinetics of the thermochemical processes were no affected by the anaerobic digestion. Finally, between the two models (DAEM and the PMSM) used to predict the weight loss curves of the pyrolysis and combustion processes, DAEM was considered to be the best model that fitted the experimental data.

## Acknowledgement

Authors acknowledge the financial support from the Regional Government of Castilla-La Mancha (Project PEII-2014-007-P) and also from the University of Castilla-La Mancha of Spain (UCLM grant).

## References

Anca-Couce, A., Berger, A., et al., 2014. How to determine consistent biomass pyrolysis kinetics in a parallel reaction scheme. Fuel 123, 230–240.
BP, 2013. BP Statistical Review of World Energy, June 2014. Available online at: bp.com/statisticalreview.
Brown, M.E., 1998. Handbook of Thermal Analysis and Calorimetry: Principles and Practice. Elsevier Science.
Cai, J., Wu, W., et al., 2013. Sensitivity analysis of three-parallel-DAEM-reaction model for describing rice straw pyrolysis. Bioresour. Technol. 132, 423–426.
Cai, J., Wu, W., et al., 2014. An overview of distributed activation energy model and its application in the pyrolysis of lignocellulosic biomass. Renew. Sustain. Energy Rev. 36, 236–246.
Cao, J.-P., Huang, X., et al., 2015. Nitrogen transformation during gasification of livestock compost over transition metal and Ca-based catalysts. Fuel 140, 477–483.
Ceylan, S., Topçu, Y., 2014. Pyrolysis kinetics of hazelnut husk using thermogravimetric analysis. Bioresour. Technol. 156, 182–188.
Coats, A.W., Redfern, J.P., 1964. Kinetic parameters from thermogravimetric data. Nature 201, 68–69.
Chen, C., Ma, X., et al., 2011. Thermogravimetric analysis of microalgae combustion under different oxygen supply concentrations. Appl. Energy 88, 3189–3196.
Damartzis, T., Vamvuka, D., et al., 2011. Thermal degradation studies and kinetic modeling of cardoon (*Cynara cardunculus*) pyrolysis using thermogravimetric analysis (TGA). Bioresour. Technol. 102, 6230–6238.
de Caprariis, B., De Filippis, P., et al., 2012. Double-Gaussian distributed activation energy model for coal devolatilization. Energy Fuels 26, 6153–6159.
Doyle, C.D., 1962. Estimating isothermal life from thermogravimetric data. J. Appl. Polym. Sci. 6, 639–642.

Fernandez-Lopez, M., Puig-Gamero, M., et al., 2015. Life cycle assessment of swine and dairy manure: pyrolysis and combustion processes. Bioresour. Technol. 182, 184–192.
Friedman, H.L., 1969. New methods for evaluating kinetic parameters from thermal analysis data. J. Polym. Sci. Pol. Lett. 7, 41–46.
Garcia-Maraver, A., Perez-Jimenez, J.A., et al., 2015. Determination and comparison of combustion kinetics parameters of agricultural biomass from olive trees. Renew. Energy 83, 897–904.
Kantarelis, E., Yang, W., et al., 2011. Thermochemical treatment of E-waste from small household appliances using highly pre-heated nitrogen-thermogravimetric investigation and pyrolysis kinetics. Appl. Energy 88, 922–929.
Kirtania, K., Bhattacharya, S., 2012. Application of the distributed activation energy model to the kinetic study of pyrolysis of the fresh water algae *Chlorococcum humicola*. Bioresour. Technol. 107, 476–481.
López-González, D., Fernandez-Lopez, M., et al., 2013. Thermogravimetric-mass spectrometric analysis on combustion of lignocellulosic biomass. Bioresour. Technol. 143, 562–574.
López-González, D., Fernandez-Lopez, M., et al., 2014. Pyrolysis of three different types of microalgae: kinetic and evolved gas analysis. Energy 73, 33–43.
Navarro, M.V., Aranda, A., et al., 2008. Application of the distributed activation energy model to blends devolatilisation. Chem. Eng. J. 142, 87–94.
Papari, S., Hawboldt, K., 2015. A review on the pyrolysis of woody biomass to bio-oil: focus on kinetic models. Renew. Sustain. Energy Rev. 52, 1580–1595.
Sharara, M.A., Holeman, N., et al., 2014. Pyrolysis kinetics of algal consortia grown using swine manure wastewater. Bioresour. Technol. 169, 658–666.
Slopiecka, K., Bartocci, P., et al., 2012. Thermogravimetric analysis and kinetic study of poplar wood pyrolysis. Appl. Energy 97, 491–497.
Sun, Y., Bai, F., et al., 2015. Kinetic study of Huadian oil shale combustion using a multi-stage parallel reaction model. Energy 82, 705–713.
Tran, K.-Q., Bach, Q.-V., et al., 2014. Non-isothermal pyrolysis of torrefied stump – a comparative kinetic evaluation. Appl. Energy 136, 759–766.
Várhegyi, G., Bobály, B., et al., 2011. Thermogravimetric study of biomass pyrolysis kinetics. A distributed activation energy model with prediction tests. Energy Fuels 25, 24–32.
Várhegyi, G., Sebestyén, Z., et al., 2012. Combustion kinetics of biomass materials in the kinetic regime. Energy Fuels 26, 1323–1335.
Vyazovkin, S., Burnham, A.K., et al., 2011. ICTAC Kinetics Committee recommendations for performing kinetic computations on thermal analysis data. Thermochim. Acta 520, 1–19.
White, J.E., Catallo, W.J., et al., 2011. Biomass pyrolysis kinetics: a comparative critical review with relevant agricultural residue case studies. J. Anal. Appl. Pyrol. 91, 1–33.
Xiao, H.-m., Ma, X.-q., et al., 2009. Isoconversional kinetic analysis of co-combustion of sewage sludge with straw and coal. Appl. Energy 86, 1741–1745.
Xu, Y., Chen, B., 2013. Investigation of thermodynamic parameters in the pyrolysis conversion of biomass and manure to biochars using thermogravimetric analysis. Bioresour. Technol. 146, 485–493.
Zhang, J., Chen, T., et al., 2015. TG-MS analysis and kinetic study for thermal decomposition of six representative components of municipal solid waste under steam atmosphere. Waste Manage. 43, 152–161.